

# Multibody Dynamics

# Computational Methods in Applied Sciences

---

Volume 23

---

## *Series Editor*

E. Oñate

International Center for Numerical Methods in Engineering (CIMNE)

Technical University of Catalunya (UPC)

Edificio C-1, Campus Norte UPC

Gran Capitán, s/n

08034 Barcelona, Spain

onate@cimne.upc.edu

www.cimne.com

For other titles published in this series, go to

[www.springer.com/series/6899](http://www.springer.com/series/6899)

Krzysztof Arczewski • Wojciech Blajer  
Janusz Frączek • Marek Wojtyra  
Editors

# Multibody Dynamics

Computational Methods and Applications

 Springer

*Editors*

Krzysztof Arczewski  
Warsaw University of Technology  
Faculty of Power and Aeronautical  
Engineering  
ul. Nowowiejska 24  
00-665 Warsaw  
Poland  
krisarcz@meil.pw.edu.pl

Janusz Frączek  
Warsaw University of Technology  
Faculty of Power and Aeronautical  
Engineering  
ul. Nowowiejska 24  
00-665 Warsaw  
Poland  
jfraczek@meil.pw.edu.pl

Wojciech Blajer  
Technical University of Radom  
Faculty of Mechanical Engineering  
ul. Krasickiego 54  
26-600 Radom  
Poland  
w.blajer@pr.radom.pl

Marek Wojtyra  
Warsaw University of Technology  
Faculty of Power and Aeronautical  
Engineering  
ul. Nowowiejska 24  
00-665 Warsaw  
Poland  
mwojtyra@meil.pw.edu.pl

ISSN 1871-3033

ISBN 978-90-481-9970-9

e-ISBN 978-90-481-9971-6

DOI 10.1007/978-90-481-9971-6

Springer Dordrecht Heidelberg London New York

Library of Congress Control Number: PCN applied for

© Springer Science+Business Media B.V. 2011

No part of this work may be reproduced, stored in a retrieval system, or transmitted in any form or by any means, electronic, mechanical, photocopying, microfilming, recording or otherwise, without written permission from the Publisher, with the exception of any material supplied specifically for the purpose of being entered and executed on a computer system, for exclusive use by the purchaser of the work.

Printed on acid-free paper

Springer is part of Springer Science+Business Media ([www.springer.com](http://www.springer.com))

# Preface

Multibody Dynamics is an exciting area of applied and computational mechanics, whose substantial progress during the last five decades has stemmed from the rapid and simultaneous development of many technological disciplines like robotics, spacecraft and machine design, and was stimulated by the advances in computational techniques. In order to deliver methods and tools for the modeling, analysis and simulation of complex mechanical systems, various topics were merged in the field, including contact and impact, control and mechatronics, real-time simulation, optimization, flexibility, time integration schemes and software development. The current area of interest include robotics and walking machines, road and railway vehicle dynamics, aerospace, biomechanics, and many other multidisciplinary applications.

The ECCOMAS Thematic Conference on Multibody Dynamics was initiated in Lisbon in 2003, and then continued in Madrid (2005) and Milan (2007), aimed at providing a venue for exchanging ideas and recent developments related to the theory and applications of multibody systems. The fourth edition of the Conference was held at the Warsaw University of Technology, Warsaw, Poland, from June 29 to July 2, 2009. At the Conference participated 219 researchers from 27 countries, mainly from Europe (162), but also from Asia (40), and North (13) and South America (4). They presented 167 technical papers, having an excellent forum for discussion and technical exchange on the most recent advances in the rapidly growing field of Multibody Dynamics.

The present book is a collection of revised and extended versions of 15 papers presented at the Conference, recommended by the Session Organizers for publication in this post-conference book. The general selection criterion was that the papers best reflect the state-of-art of the topics associated to the particular sessions, and cover the areas of biomechanics (Raison et al.), contact dynamics (Flores et al./Ziegler and Eberhard), control, mechatronics and robotics (Iwamura et al./Seifried), efficient methods and real-time applications (Cavagna et al./Pfau and Schaden), flexible multibody dynamics (Ambrósio et al./Dibold and Gerstmayr), formulations and numerical methods (García Orden and Aguilera/Schindler et al.), miscellaneous multibody applications (Frączek and Wojtyra), optimization

(Brüls et al.), software development, validation, and education (Tasora et al.), and vehicle systems (Bottasso et al.). We hope you will find the reading of this collection enjoyable and stimulating.

March 2010  
Radom/Warsaw

Wojciech Blajer, Krzysztof Arczewski  
Janusz Frączek, and Marek Wojtyra

# Contents

<b>A Flexible Multibody Pantograph Model for the Analysis of the Catenary–Pantograph Contact</b> .....	1
Jorge Ambrósio, Frederico Rauter, João Pombo, and Manuel S. Pereira	
<b>Maneuvering Multibody Dynamics: New Developments for Models with Fast Solution Scales and Pilot-in-the-Loop Effects</b> .....	29
Carlo L. Bottasso, Giorgio Maisano, and Francesco Scorcelletti	
<b>Optimization of Multibody Systems and Their Structural Components</b> .....	49
Olivier Brüls, Etienne Lemaire, Pierre Duysinx, and Peter Eberhard	
<b>Real-Time Aeroservoelastic Analysis of Wind-Turbines by Free Multibody Software</b> .....	69
Luca Cavagna, Alessandro Fumagalli, Pierangelo Masarati, Marco Morandini, and Paolo Mantegazza	
<b>Comparison of Planar Structural Elements for Multibody Systems with Large Deformations</b> .....	87
Markus Dibold and Johannes Gerstmayr	
<b>Modeling and Analysis of Rigid Multibody Systems with Translational Clearance Joints Based on the Nonsmooth Dynamics Approach</b> .....	107
Paulo Flores, Remco Leine, and Christoph Glocker	
<b>Application of General Multibody Methods to Robotics</b> .....	131
Janusz Frączek and Marek Wojtyra	

<b>Energy Considerations for the Stabilization of Constrained Mechanical Systems with Velocity Projection</b> .....	153
Juan C. García Orden and Roberto A. Ortega Aguilera	
<b>A General Purpose Algorithm for Optimal Trajectory Planning of Closed Loop Multibody Systems</b> .....	173
Makoto Iwamura, Peter Eberhard, Werner Schiehlen, and Robert Seifried	
<b>Real-Time Simulation of Extended Vehicle Drivetrain Dynamics</b> .....	195
Ralf U. Pfau and Thomas Schaden	
<b>Assessment of Antagonistic Muscle Forces During Forearm Flexion/Extension</b> .....	215
Maxime Raison, Christine Detrembleur, Paul Fisette, and Jean-Claude Samin	
<b>Computing Time Reduction Possibilities in Multibody Dynamics</b> .....	239
Thorsten Schindler, Markus Friedrich, and Heinz Ulbrich	
<b>Optimization-Based Design of Minimum Phase Underactuated Multibody Systems</b> .....	261
Robert Seifried	
<b>GPU-Based Parallel Computing for the Simulation of Complex Multibody Systems with Unilateral and Bilateral Constraints: An Overview</b> .....	283
Alessandro Tasora, Dan Negrut, and Mihai Anitescu	
<b>Investigation of Gears Using an Elastic Multibody Model with Contact</b> .....	309
Pascal Ziegler and Peter Eberhard	



# A Flexible Multibody Pantograph Model for the Analysis of the Catenary–Pantograph Contact

Jorge Ambrósio, Frederico Rauter, João Pombo, and Manuel S. Pereira

**Abstract** The pantograph–catenary system is still the most reliable form of collecting electric energy for running trains. This system should ideally run with relatively low contact forces, in order to minimize wear and damage of the contacting elements but without contact loss to avoid power supply interruption and electric arching. However, the quality of the pantograph–catenary contact may be affected by operational conditions, defects on the overhead equipment, environmental conditions or by the flexibility of the pantograph components. In this work a flexible multibody methodology based on the use of the mean-axis conditions, as reference conditions, mode component synthesis, as a form of reducing the number of generalized coordinates of the system and virtual bodies, as a methodology to allow the use of all kinematic joints available for multibody modeling and application of external forces, are used to allow building the flexible multibody pantograph models. The catenary model is built in a linear finite element code developed in a Matlab environment, which is co-simulated with the multibody code to represent the complete system interaction. A thorough description of rigid-flexible multibody pantograph models is presented in a way that the proposed methodology can be used. Several flexible multibody models of the pantograph are described and proposed and the quality of the pantograph–catenary contact is analyzed and discussed in face of the flexibility of the overhead components.

## 1 Introduction

The interaction between the pantograph and the catenary is one of the factors that limits the operating speed of railway vehicles and, consequently, is one of the research priorities in the European railway community. These limitations

---

J. Ambrósio (✉), F. Rauter, J. Pombo, and M.S. Pereira  
IDMEC-IST, Av. Rovisco Pais 1, Lisboa, Portugal  
e-mail: [jorge@dem.ist.utl.pt](mailto:jorge@dem.ist.utl.pt); [frauter@dem.ist.utl.pt](mailto:frauter@dem.ist.utl.pt); [jpombo@dem.ist.utl.pt](mailto:jpombo@dem.ist.utl.pt);  
[mpereira@dem.ist.utl.pt](mailto:mpereira@dem.ist.utl.pt)

concern not only the ability to collect energy at high operating speeds but also the interoperability between the overhead equipment in trains and infrastructure. From the mechanical point of view, the most important feature of the pantograph–catenary system consists on the contact quality between the registration strips of the pantograph and the contact wires of the catenary. The system must ideally run with relatively low contact forces, to minimize wear and damage of the contact elements, but with high enough contact forces to prevent contact loss, to ensure a constant power supply and minimize the occurrence of electric arching. The design of pantograph–catenary systems aims at controlling the interaction phenomena maintaining the contact forces within an acceptable operational envelope. Among the factors that affect the quality of the pantograph–catenary contact are those concerned with the defects on the catenary or pantograph, environmental conditions, such as wind [1, 2] and extreme temperatures [3], running dynamics of the railway vehicle and the deformability of the pantograph mechanical system. This work proposes the use of flexible multibody methodologies to describe the pantograph system and the co-simulation of the models obtained with detailed finite element models of the catenary to evaluate the quality of the overhead contact and to identify the main mechanical issues influencing it.

Some of the earlier works in flexible multibody systems use fixed reference frames to describe the small elastic deformations given by the finite element method of planar mechanical systems [4]. This methodology effectively coupled the rigid body motion and the small deformations. To be able to analyze complex shaped flexible multibody systems, Shabana and Wehage proposed the use of substructuring and the model component synthesis method to reduce the number of generalized coordinates required to represent the flexible components [5, 6]. Reduction of the dimension of the flexible multibody problem is achieved by choosing only a small number of suitable vibration modes. In most cases only a small number of natural modes of vibration are needed, namely those related to the lower natural frequencies of the structure. The static correction modes represent the typical response of a structure subject to given boundary conditions [7]. Criteria to estimate the number of modes of vibration of each type have been proposed and proven to be successful for low velocity systems [8].

The coupling terms is dependent of the type of finite elements used in the model and involve the derivation of the element shape functions, which are not available in finite element literature [9, 10]. To enable the general use of finite element types in the analysis of flexible multibody systems a lumped mass formulation, based on the diagonalization of the mass matrix preserving the rotational inertia, is used [11].

For problems in which the flexible bodies experience nonlinear deformation the approach must be different and based on large displacements and rotations theory [12–14]. For nonlinear problems Kane and coworkers propose a nonlinear theory that includes the dynamic stiffening [15]. In the line of work developed by the finite element community [16–18], Cardona and Geradin propose a formulation for the nonlinear flexible bodies using either exact geometrical models or substructuring [19, 20]. An approach based on the use of the finite rotations nodal coordinates enabling the capture of the geometric nonlinear deformations has been proposed

and named absolute nodal coordinates [21]. A different approach has been proposed to model geometric nonlinear deformations based on relaxing the need to exhibit small moderate rotations about the reference frame, by using an incremental finite-element approach within the flexible body description [22]. The extent of the use of the referred approach to model material nonlinearities has also been proposed [23]. In these formulations the rigid body motion and the elastic variables are expressed in inertia reference frames, where the deformation state is derived with respect to local reference frames and a relation deformation-displacement is obtained but, due to the inherent nonlinearity of the deformations, the problem cannot be reduced implying the handling of large system matrices during the analysis process. Because the deformations observed in the pantograph or on the catenary are small, only linear elastodynamics is considered in the flexible multibody models used. In any case, structural damping is used in order to improve the time integration [24].

The use of finite element method on the framework of flexible multibody dynamics implies the definition of a set of reference conditions. Straightforward reference conditions are the body fixed reference frames, where the frame is attached to one or more nodes of the flexible body, constraining at least six degrees of freedom [11]. The mean-axis reference conditions correspond to a different approach by introducing a floating frame defined to minimize the kinetic energy associated to the deformation, measured with respect to an observer stationed on the flexible body [25, 26]. Another type of floating reference frame is called the principal axis reference conditions where the origin of the reference frame is associated to the instantaneous center of mass and its directions to the principal inertia directions [27]. Augusta and Ambrósio analyze and point out the major advantages and drawbacks of the different methodologies and their main applications [28]. The mean-axis conditions are used here as reference conditions for the flexible multibody formulation.

To be able to use the extensive library of kinematic constraints developed for rigid multibody systems with flexible bodies, the concept of virtual bodies has been developed [29, 30]. The numerical efficiency of this methodology applied to complex structures was shown using a sparse matrix solver after comparison to that of multibody models with custom developed flexible kinematic joints [31]. Kinematic joints based on the use of the virtual body approach [32] are implemented in this work so that the pantograph model can include the type of kinematic joints particular to its construction, described in reference [32].

Previous studies of the catenary–pantograph interaction emphasized not only the mechanical aspects of construction, operation and maintenance but also the challenges of its numerical simulation due to the multi-physics characteristic of this problem. Ranging from simple linear catenary models using 2D finite elements [33], or having the catenary represented by cables and loaded by a lumped mass model of a pantograph [34] several approaches proposed kept the problem simple enough to tackle it by a single code. In a similar line of work Dahlberg describes the contact wire as an axially loaded beam and uses modal analysis to represent its deflection when subjected to transversal and axial loads, showing in the process its relation to the critical velocity of the pantograph [35]. Labergri presents a very thorough description of the pantograph–catenary system that includes a 2D

finite element model for the catenary and a multibody pantograph, being the contact treated by unilateral constraints [36]. In all works mentioned it is claimed that the catenary structural deformations are basically linear and consequently the catenary systems are modeled using linear finite elements. The slacking of droppers is an exception being handled as a nonlinear effect. Another approach is proposed by Seo and coworkers that states the need to treat the catenaries as being nonlinear due to their large deformations [37, 38]. The large deformation of the catenary is modeled using the three-dimensional finite element absolute nodal coordinate formulation while the pantograph is a full 3D multibody model. The interaction between the pantograph and the catenary is modeled by a sliding joint that allows for the motion of the pan-head on the catenary cable and no contact loss is represented [38]. Arnold and Simeon address the pantograph–catenary interaction as time dependent problems coupled by constraints on boundaries [39]. A half-explicit integration method reversible in time was also developed in order to preserve as much information as possible during time discretization. Due to the multi-physics problem involved in the catenary–pantograph system, Veitl and Arnold proposed a co-simulation strategy between the code PROSA, where a catenary is described by the finite difference method and the SIMPACK commercial multibody code, used to simulate the pantograph [40]. Several strategies tackling the co-simulation problem, such as gluing algorithms proposed by Hulbert and coworkers [41] or the co-simulation procedures suggested by Kubler and Schiehlen [42]. Recognizing that the finite element method is appropriate to model in detail the catenary and that the multibody dynamics approach is suited to handle the pantograph dynamics, a co-simulation approach using two separate codes is proposed in this work.

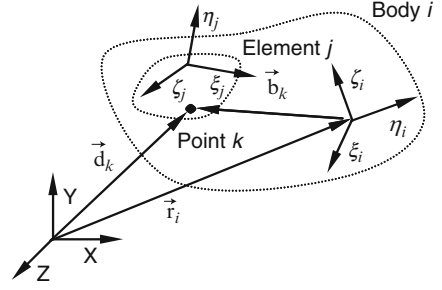
## 2 Flexible Multibody Systems

### 2.1 Flexible Body Equations of Motion

For the flexible body depicted by Fig. 1 let  $\mathbf{q}_i = [\mathbf{q}_r^T \mathbf{u}'^T]^T$  be the vector of generalized coordinates of body  $i$ , where  $\mathbf{q}_r = [\mathbf{r}_i^T \mathbf{p}_i^T]^T$  represents the translational and rotational position of body  $i$  local coordinate system  $(\xi, \eta, \zeta)_i$  and vector  $\mathbf{u}'$  represents body  $i$  elastic coordinates. The flexible body equations of motion are obtained by Gonçalves and Ambrósio as [11].

$$\begin{bmatrix} \mathbf{M}_{rr} & \mathbf{M}_{r\phi} & \mathbf{M}_{rf} \\ \mathbf{M}_{\phi r} & \mathbf{M}_{\phi\phi} & \mathbf{M}_{\phi f} \\ \mathbf{M}_{fr} & \mathbf{M}_{f\phi} & \mathbf{M}_{ff} \end{bmatrix}_i \begin{bmatrix} \ddot{\mathbf{r}}_i \\ \dot{\omega}'_i \\ \ddot{\mathbf{u}}'_i \end{bmatrix} = \begin{bmatrix} \mathbf{g}_r \\ \mathbf{g}'_\phi \\ \mathbf{g}'_f \end{bmatrix}_i + \begin{bmatrix} \mathbf{s}_r \\ \mathbf{s}'_\phi \\ \mathbf{s}'_f \end{bmatrix}_i - \begin{bmatrix} \mathbf{0} & \mathbf{0} & \mathbf{0} \\ \mathbf{0} & \mathbf{0} & \mathbf{0} \\ \mathbf{0} & \mathbf{0} & \mathbf{K}_i \end{bmatrix} \begin{bmatrix} \mathbf{r}_i \\ \mathbf{p}_i \\ \mathbf{u}'_i \end{bmatrix} \quad (1)$$

where the mass matrix  $\mathbf{M}_i$  contains the mass, inertia tensor and inertia coupling terms, vector  $\mathbf{s}_i$  represents the velocity quadratic terms and other acceleration independent terms,  $\mathbf{g}_i$  is the generalized external force vector, and  $\mathbf{K}_i$  is the finite

**Fig. 1** Flexible body  $i$ 


elements stiffness matrix. The mass matrix in Eq. (1) may be either consistent or lumped. In order to maintain the inertia coupling terms independent of the finite element shape functions, the lumped mass formulation is used in this work [11].

The equations of motion obtained, using consistent or diagonalized mass matrices, do not have a unique displacement field. It is necessary to impose a set of reference conditions to eliminate the rigid body modes and provide the unique displacement field of the flexible body. In general, reference conditions are written as kinematic constraints that relate the independent and the dependent elastic coordinates. The mean axis conditions constraints are such that enforce the local frame  $(\xi, \eta, \zeta)_i$  of body  $i$  to follow the motion of the nodes in such a way that the kinetic energy associated with the deformation corresponds to a minimum value for an observer stationary in the body local frame [25, 26]. The deformation kinetic energy of a flexible body can be expressed in terms of the generalized elastic coordinates with respect to the local coordinate system  $(\xi, \eta, \zeta)_i$  as:

$$T = \frac{1}{2} \dot{\mathbf{u}}'^T \mathbf{M} \dot{\mathbf{u}}' = \frac{1}{2} \sum_{k=1}^n m_k \dot{\delta}_k'^T \dot{\delta}_k' + \frac{1}{2} \sum_{k=1}^n \dot{\theta}_k'^T \boldsymbol{\mu}_k \dot{\theta}_k' \quad (2)$$

where the nodal translation velocities are denoted by  $\dot{\delta}_k'$  and the nodal angular velocities by  $\dot{\theta}_k'$ . The generalized elastic coordinate velocities  $\dot{\mathbf{u}}'_k$  of a node  $k$  of the body mesh are written in terms of generalized set of coordinates  $\mathbf{q}_r$  of the body as:

$$\dot{\mathbf{u}}'_k = \begin{bmatrix} \dot{\delta}_k' \\ \dot{\theta}_k' \end{bmatrix} = \begin{bmatrix} \mathbf{A}^T (\dot{\mathbf{d}}_k - \dot{\mathbf{r}} + \mathbf{A} \tilde{\mathbf{b}}'_k \boldsymbol{\omega}') \\ \dot{\boldsymbol{\alpha}}'_k - \boldsymbol{\omega}' \end{bmatrix} \quad (3)$$

in which matrix  $\mathbf{A}$  represents the transformation matrix from the body local coordinate system to the inertial frame. Minimizing the deformation kinetic energy of the body with respect to the translational and rotational velocities leads to

$$T_{\dot{\mathbf{r}}} = \frac{\partial T}{\partial \dot{\mathbf{r}}} = \sum_{k=1}^n m_k (\dot{\mathbf{d}}_k - \dot{\mathbf{r}} + \mathbf{A} \tilde{\mathbf{b}}'_k \boldsymbol{\omega}') = 0$$

$$T_{\boldsymbol{\omega}'} = \frac{\partial T}{\partial \boldsymbol{\omega}'} = \sum_{k=1}^n m_k (\mathbf{A} \tilde{\mathbf{b}}'_k)^T (\dot{\mathbf{d}}_k - \dot{\mathbf{r}} + \mathbf{A} \tilde{\mathbf{b}}'_k \boldsymbol{\omega}') + \sum_{k=1}^n \boldsymbol{\mu}_k (\dot{\boldsymbol{\alpha}}'_k - \boldsymbol{\omega}') = 0 \quad (4)$$

Substituting Eq. (3) into Eq. (4) results in the velocity constraint equations that define the mean axis reference conditions, as

$$\dot{\Phi}^{(ma)} \equiv \left\{ \begin{array}{c} \sum_{k=1}^n m_k \dot{\delta}'_k \\ \sum_{k=1}^n m_k \tilde{\mathbf{b}}_k'^T \dot{\delta}'_k + \sum_{k=1}^n \mu_k \dot{\theta}'_k \end{array} \right\} = \mathbf{0} \quad (5)$$

The velocity constraint equations may be written in more compact form as:

$$\dot{\Phi}^{(ma)} \equiv \Phi_{\mathbf{u}'}^{(ma)} \dot{\mathbf{u}}' = \mathbf{0} \quad (6)$$

where  $\Phi_{\mathbf{u}'}^{(ma)}$  represents the Jacobian matrix of the mean axis reference conditions constraint equations, which is explicitly written as

$$\Phi_{\mathbf{u}'}^{(ma)} = \begin{bmatrix} \Phi_{\delta'}^{(ma)} \\ \Phi_{\theta'}^{(ma)} \end{bmatrix} = \begin{bmatrix} \sum_{k=1}^n m_k \mathbf{I}_k^T & \mathbf{0}^T \\ \sum_{k=1}^n m_k \tilde{\mathbf{b}}_k' \mathbf{I}_k^T & \sum_{k=1}^n \mu_k \mathbf{I}_k^T \end{bmatrix} \quad (7)$$

The time derivative of Eq. (6) results in the acceleration constraint equations of the mean axis reference conditions, written here in a compact form as

$$\ddot{\Phi}^{(ma)} \equiv \Phi_{\mathbf{u}'}^{(ma)} \ddot{\mathbf{u}}' = \boldsymbol{\gamma}^{(ma)} \quad (8)$$

The constraints associated to the mean axis conditions are imposed on the flexible body equations of motion, described by Eq. (1), leading to

$$\begin{bmatrix} \mathbf{M}_r & \mathbf{0} & \mathbf{0} \\ \mathbf{M}_{fr} & \mathbf{M}_{ff} & \Phi_{\mathbf{u}'}^{(ma)T} \\ \mathbf{0} & \Phi_{\mathbf{u}'}^{(ma)} & \mathbf{0} \end{bmatrix} \begin{bmatrix} \ddot{\mathbf{q}}_r \\ \ddot{\mathbf{u}}' \\ \boldsymbol{\lambda}^{(ma)} \end{bmatrix} = \begin{bmatrix} \mathbf{g}_r \\ \mathbf{g}'_f \\ \boldsymbol{\gamma}^{(ma)} \end{bmatrix} - \begin{bmatrix} \mathbf{s}_r \\ \mathbf{s}'_f \\ \mathbf{0} \end{bmatrix} - \begin{bmatrix} \mathbf{0} \\ \mathbf{K}_f \mathbf{u}' \\ \mathbf{0} \end{bmatrix} \quad (9)$$

Note that the mean axis conditions are non-holonomic constraint conditions and can only be defined at the velocity and acceleration levels.

The flexible body equations of motion, shown in Eq. (9), include a very large number of generalized coordinates, leading to a computational expensive procedure. For linear elastic small deformations, as those experienced by the pantograph components in the applications foreseen in this work, it is possible to represent the deformation of the flexible body as a sum of deformation modes that are constant in time. Let those deformation modes be the modes of vibration associated to the natural frequencies of the flexible body. The generalized elastic coordinates of body  $i$  are now described by a weighted sum of these modes as

$$\mathbf{u}' = \mathbf{X}\mathbf{w} \quad (10)$$

where  $\mathbf{w}$  represents the contributions of the modes of vibration towards the nodal displacements and  $\mathbf{X}$  the modal matrix containing a selected number of modes of vibration  $\chi_i$  that are obtained by solving the eigenproblem:

$$\mathbf{K}_{ff}\chi_i = \bar{\omega}_i \mathbf{M}_{ff}\chi_i \quad (11)$$

The solution of Eq. (11) is independent of the reference conditions used to constrain the rigid body movement of the elastic coordinates. Therefore the modes of vibration obtained correspond to those of a structure free in space, defined as free-free modes. The vibration modes obtained related to the first six lowest frequencies, generally null, represent the rigid body motion of the flexible body. These modes of vibration are removed from the modal matrix. A simpler system of equations is obtained by normalizing  $\chi_i$  with respect to the mass matrix  $\mathbf{M}_{ff}$

$$\mathbf{X}^T \mathbf{M}_{ff} \mathbf{X} = \mathbf{I} \quad (12)$$

$$\mathbf{X}^T \mathbf{K}_{ff} \mathbf{X} = \mathbf{\Lambda} \quad (13)$$

where  $\mathbf{\Lambda}$  is a diagonal matrix containing the square the natural frequencies associated to each mode of vibration.

By substituting Eq. (10), and its time derivatives, into Eq. (9), pre-multiplying the second row by  $\mathbf{X}^T$  and using the relations described by Eqs. (12) and (13) leads to:

$$\begin{bmatrix} \mathbf{M}_r & \mathbf{M}_{rf}\mathbf{X} & \Phi_{q_r}^T \\ \mathbf{X}^T \mathbf{M}_{fr} & \mathbf{I} & \mathbf{X}^T \Phi_{q_f}^T \\ \Phi_{q_r} & \Phi_{q_f} \mathbf{X} & \mathbf{0} \end{bmatrix} \begin{bmatrix} \ddot{\mathbf{q}}_r \\ \ddot{\mathbf{w}} \\ \lambda \end{bmatrix} = \begin{bmatrix} \mathbf{g}_r \\ \mathbf{X}^T \mathbf{g}'_f \\ \gamma \end{bmatrix} - \begin{bmatrix} \mathbf{s}_r \\ \mathbf{X}^T \mathbf{s}'_f \\ \mathbf{0} \end{bmatrix} - \begin{bmatrix} \mathbf{0} \\ \mathbf{\Lambda} \mathbf{w} \\ \mathbf{0} \end{bmatrix} \quad (14)$$

The number of generalized elastic coordinates used in Eq. (14) is equal to the number of vibration modes included in the modal matrix, thus being possible to reduce considerably the problem dimension considering a general use of flexible multibody models. The effects of local deformations induced by high concentrated loads originated, for example, by kinematic constraint reaction forces or other force elements, can also be included in the modal synthesis using of static correction modes [7, 8].

## 2.2 Kinematic Joints with Virtual Bodies

The use of flexible bodies requires that the kinematic joints implemented in the multibody code are re-written again for the new set of generalized coordinates used. A form to circumvent this difficulty is to use the concept of virtual bodies introduced by Bae et al. [30] and further developed by Ambrosio and Gonçalves [31, 32]. With the virtual body approach, a rigid joint between a flexible body and a rigid body is derived for a node  $k$  of the mesh of the flexible body and the origin of the virtual rigid body fixed reference frame, as depicted in Figs. 2 and 3. Afterwards, any

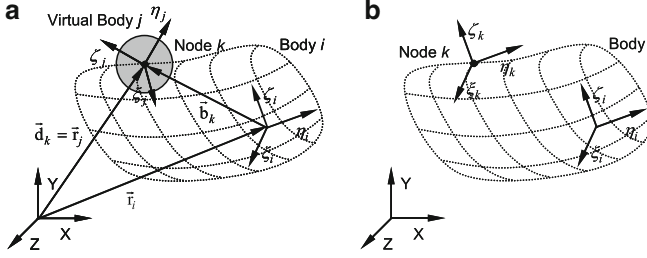


**Fig. 2** Rigid joint between a flexible body  $i$  and a massless rigid body  $j$ : (a) virtual body; (b) nodal and body fixed coordinate systems

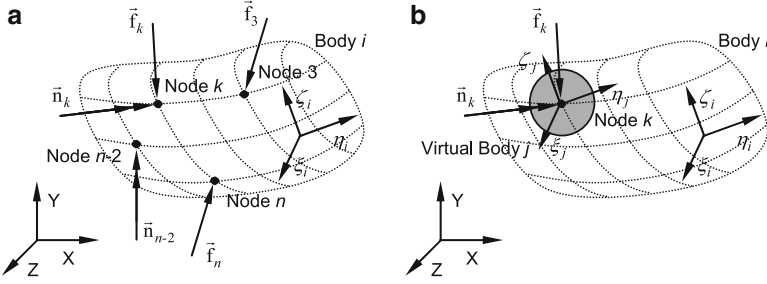


**Fig. 3** External forces applied on a flexible body: (a) Forces applied directly on the nodes; (b) FORCES applied on the virtual body attached to the finite element nodes

kinematic joint between the flexible body and other bodies of the system is established using the virtual body instead, making possible to use any of the kinematic joints available on the multibody code library.

The constraint equations for the rigid joint are defined for the translational and rotational parts of the constraint independently. Let a spherical joint be defined between node  $k$  of flexible body  $i$  and a point  $P$  of the rigid body  $j$ , coincident to the origin of the body fixed coordinate system. This is the translation part of the rigid kinematic joint written as

$$\Phi^{(t)} \equiv \mathbf{r}_j - \mathbf{r}_i - \mathbf{A}_i \mathbf{b}_k = \mathbf{0} \quad (15)$$

In order to define the rotational part of the rigid joint let a coordinate system  $(\xi, \eta, \zeta)_k$  be attached to node  $k$ , as showed in Fig. 3b. The nodal frame is defined by unit vectors  $\bar{\mathbf{e}}_k = [\bar{\mathbf{e}}_k^1 \ \bar{\mathbf{e}}_k^2 \ \bar{\mathbf{e}}_k^3] \equiv \mathbf{I}$  initially parallel to the flexible body  $i$  local reference frame  $(\xi, \eta, \zeta)_i$  unit vectors  $\mathbf{e}'_i$ . Unit vectors defining both nodal and body coordinate frames are expressed in the inertial frame  $(X, Y, Z)$  as:

$$\mathbf{e}_k = \mathbf{A}_i \mathbf{A}_k \bar{\mathbf{e}}_k \quad (16)$$

$$\mathbf{e}_j = \mathbf{A}_j \mathbf{e}'_j \quad (17)$$



where  $\mathbf{A}_k = \mathbf{I} + \tilde{\theta}'_k$  represents the nodal rotational matrix for small rotations. The rotational part of the rigid joint constraint enforces that the relative orientation between the node and virtual body reference frames remains invariant, i.e.

$$\Phi^{(r)} \equiv (\mathbf{A}_i \mathbf{A}_k \tilde{\mathbf{e}}_k^m)^T \mathbf{A}_j \mathbf{e}_j^l - \beta^{ml} = \mathbf{0}; \text{ with } (m, l) = (2, 1), (3, 1), (2, 3) \quad (18)$$

in which only three equations are defined, corresponding to the independent rotational constraints. Constants  $\beta^{ml}$  are related to the initial angle between the axis of the coordinate systems in the undeformed state.

The external applied forces on the flexible bodies are applied to the nodes of the finite element model, as shown in Fig. 3a. Assume that force  $\mathbf{f}_i$  and a moment  $\mathbf{n}_i$ , shown in Fig. 3a, are applied in node  $k$  of the flexible body. Then, introducing a virtual body rigidly attached to that node allows for the direct applications of these forces on the center of mass, as shown in Fig. 3b. Note that the use of the virtual body approach allows for setting rigid joints with more than one node at a time. This approach can be used to setup complex interaction conditions between the flexible body and the external environment.

### 3 Co-simulation of Multibody and Finite Element Codes

The fundamental element of the co-simulation between a finite element code, denominated by EUROPACAS-FE, and the multibody code, herein denominated by EUROPACAS-MB, is the contact module between the two subsystems. The contact force due to pantograph–catenary interaction is characterized by a high-frequency oscillating force with high relative amplitude. Railway industry measurement data shows that reasonable values for the contact force are, for a train running at approximately 80 m/s: a mean value of 200 N oscillating between 400 and 100 N. Loss of contact in particular points of the catenary may also occur. Therefore impact effects must be included in the model.

Most continuous force contact force models have similar features, i.e., they evaluate the contact force as a function of a pseudo-penetration between two elements and a proportionality factor often designated as stiffness of the contact elements. The contact model used here, proposed by Lankarani and Nikravesh [43], is of the Hertzian type and includes internal damping and relates the normal contact force  $f_n$  with the penetration between two rigid bodies  $\delta$  by

$$f_n = K \delta^n \left[ 1 + \frac{3(1-e^2)}{4} \frac{\dot{\delta}}{\dot{\delta}^{(-)}} \right] \quad (19)$$

where  $K$  is the generalized stiffness,  $e$  is the restitution coefficient,  $\dot{\delta}$  is the relative penetration velocity and  $\dot{\delta}^{(-)}$  is the relative impact velocity. Factor  $K$  is obtained from the Hertz contact theory as the external contact between two cylinders with perpendicular axis.

The issue of the co-simulation is now ‘reduced’ to be able to find the state variables of the finite element catenary model and of the multibody pantograph model at the same instants of time, so that the contact force and its application points can be evaluated and used in the equations of motion of each subsystem.

### 3.1 Integration of the Finite Elements Equations of Motion

The motion of the catenary is characterized by small rotations and small deformations, in which the only nonlinear effect is the slacking of the droppers, being typically modeled with linear finite elements. All catenary elements, contact and messenger wires are modeled by using Euler–Bernoulli beams. Using the finite element method, the equilibrium equations for the structural system are [44]

$$\mathbf{M} \mathbf{a} + \mathbf{C} \mathbf{v} + \mathbf{K} \mathbf{x} = \mathbf{f} \quad (20)$$

where  $\mathbf{M}$ ,  $\mathbf{C}$  and  $\mathbf{K}$  are the finite element global mass, damping and stiffness matrices of the finite element model of the catenary, not to be confused with the finite element models of the flexible bodies used for the pantograph. The nodal displacements vector is  $\mathbf{x}$  while  $\mathbf{v}$  is the vector of nodal velocities,  $\mathbf{a}$  is the vector of nodal accelerations and  $\mathbf{f}$  is the vector with the applied forces. Equation (20) is solved for  $\mathbf{x}$  or for  $\mathbf{a}$  depending on the integration method used.

In this work the integration of the nodal accelerations uses a Newmark family integration algorithm [45]. The contact forces are evaluated for  $t + \Delta t$  based on the position and velocity predictions for the FE mesh and on the pantograph predicted position and velocity. The finite element mesh accelerations are calculated by

$$(\mathbf{M} + \gamma \Delta t \mathbf{C} + \beta \Delta t^2 \mathbf{K}) \mathbf{a}_{t+\Delta t} = \mathbf{f}_{t+\Delta t} - \mathbf{C} \tilde{\mathbf{v}}_{t+\Delta t} - \mathbf{K} \tilde{\mathbf{d}}_{t+\Delta t} \quad (21)$$

Predictions for new positions and velocities of the nodal coordinates of the linear finite element model of the catenary are found as

$$\tilde{\mathbf{d}}_{t+\Delta t} = \mathbf{d}_t + \Delta t \mathbf{v}_t + \frac{\Delta t^2}{2} (1 - 2\beta) \mathbf{a}_t \quad (22a)$$

$$\tilde{\mathbf{v}}_{t+\Delta t} = \mathbf{v}_t + \Delta t (1 - \gamma) \mathbf{a}_t. \quad (22b)$$

Then, with the acceleration  $\mathbf{a}_{t+\Delta t}$  the positions and velocities of the finite elements at time  $t + \Delta t$  are corrected by

$$\mathbf{d}_{t+\Delta t} = \tilde{\mathbf{d}}_{t+\Delta t} + \beta \Delta t^2 \mathbf{a}_{t+\Delta t} \quad (23a)$$

$$\mathbf{v}_{t+\Delta t} = \tilde{\mathbf{v}}_{t+\Delta t} + \gamma \Delta t \mathbf{a}_{t+\Delta t}. \quad (23b)$$

This procedure is repeated until convergence is reached for a given time step.

### 3.2 Integration of the Multibody Equations of Motion

The forward dynamic analysis of a multibody system requires that the position vector  $\mathbf{q}^0$  and the velocity vector  $\dot{\mathbf{q}}^0$  are given. The multibody equations of motion assembled and solved for the unknown accelerations, which are in turn integrated in time together with the velocities. Due to the long periods of analysis and to the structure of the equilibrium equations not only the stabilization of the integration must be insured but also the constraint violations must be eliminated. In this work, the Baumgarte constraint stabilization method is used to stabilize the multibody system equations of motion and the Coordinate Partition Method is used to correct the position and velocity constraint equations when the violations exceed a prescribed acceptable tolerance [46], as depicted in Fig. 4.

The pantograph–catenary system is characterized by an intermittence of the contact between the contact wire of the catenary and the registration strip of the pantograph. The numerical methods used for the dynamic simulation must be able to represent the loss and start of contact. This fact puts particular restrictions on the numerical integration algorithms for both pantograph and catenary with particular emphasis on the time step size selection. The multibody code used for the pantograph dynamics, considered here, uses as a Gear multi-step multi-order integration algorithm [47, 48].

### 3.3 Co-simulation Using Different Codes

The analysis of the pantograph–catenary interaction is done by two independent codes, the pantograph code, EUROPACAS-MB, which uses a multibody

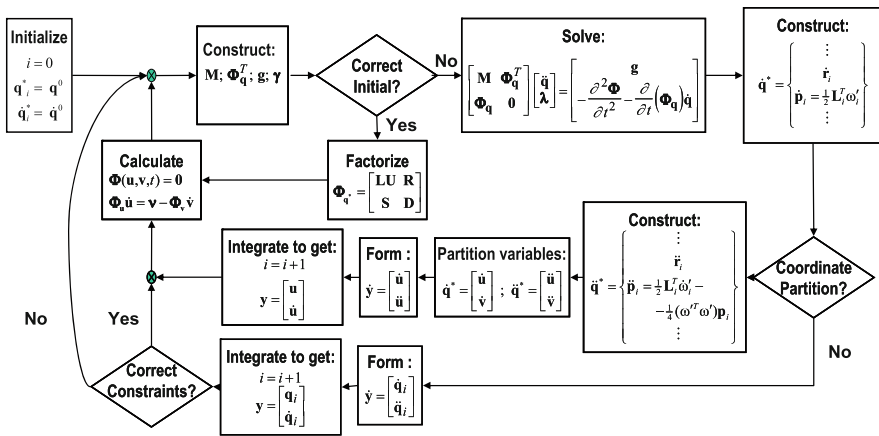


Fig. 4 Flowchart representing the forward dynamic analysis of a multibody system implemented

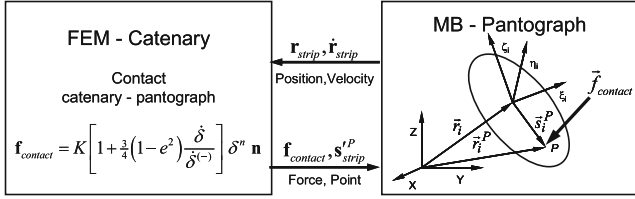


Fig. 5 Structure of the communication scheme between the MB and the FE codes

formulation, and the catenary code, EUROPACAS-FE that is a finite element software. Both programs can work as stand-alone codes. The EUROPACAS-MB code provides the EUROPACAS-FE code with the positions and velocities of the pantographs registration strips. EUROPACAS-FE calculates the contact force, using the contact model represented by Eq. (19), and the location of the application points in the pantographs and catenary, using geometric interference. These forces are applied to the catenary, in the finite element code, and to the pantograph model, in the MB code, as implied in Fig. 5. Each code handles separately the equations of motion of each sub-system based on the shared force information.

The compatibility between the two integration algorithms imposes that the state variables of the two subsystems are readily available during the integration time but also that a reliable prediction of the contact forces is also available at any given time step. Several strategies can be envisaged to tackle this co-simulation problem such as the gluing algorithms proposed by Hulbert et al. [41] or the co-simulation procedures suggested by Kubler and Schiehlen [42]. The key of the synchronization procedure between the MB and FE codes is the time integration, which must be such that it is ensured the correct dynamic analysis of the pantograph–catenary system, including the loss and regain of contact. Let it be assumed that the FE integration code is of the Newmark family and has a constant time step. Moreover, let it be assumed that the time step of the FE is small enough not only to assure the stability of the integration of the catenary but also to be able to capture the initiation of the contact between the pantograph registration strip and the contact wire of the catenary. The only restriction that is imposed in the integration algorithm of the multibody code is that its time step cannot exceed the time step of the FE code. Finally let it be assumed that both codes can start independently from each other, i.e., the catenary FE model and the pantograph MB model include the initial conditions for the start of the analysis expressed in terms of the initial positions and velocities of all components of the systems. A fully integrated communication interface is implemented according to the two stages represented in Fig. 6.

Initially, when both codes exchange input data information, it is necessary to perform initialization procedures, while, after, data is shared during the dynamic analysis [49, 50]. The EUROPACAS-MB code provides the EUROPACAS-FE code with the information about the number of contacting bodies in the model, and their initial position and velocity. Subsequently, the EUROPACAS-FE code provides the MB code with information about the initial and final analysis time and the time step

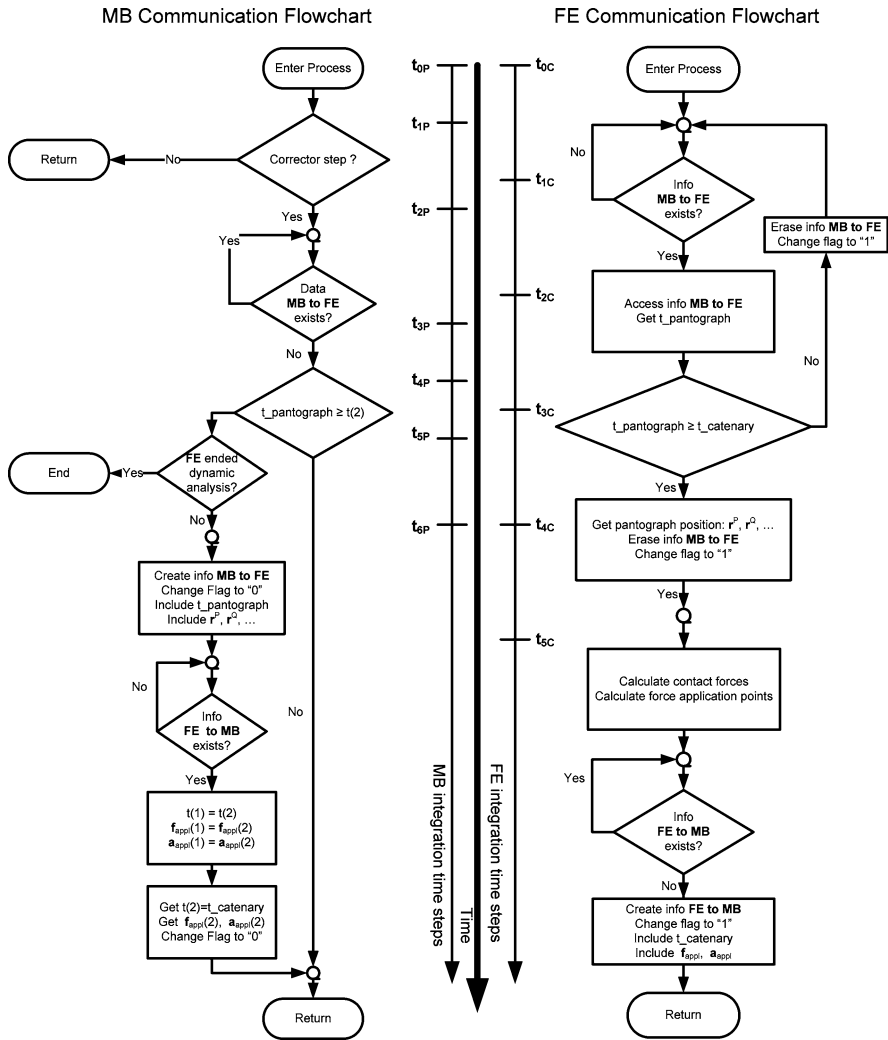


Fig. 6 Communication procedure during the dynamic analysis

to be used in the FE analysis. Note that nowhere in the communication procedure outlined it is implied what kind of integration algorithm is used for the FE catenary analysis, provided that it is a fixed time step integrator. Even this condition can be relaxed, but it would not have any practical implication as it is not usual that FE dynamic analysis is performed with variable time step integrators.

## 4 Analysis of the Pantograph–Catenary Contact Problem

### 4.1 Pantograph Multibody Models

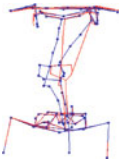
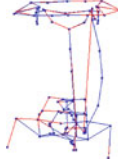
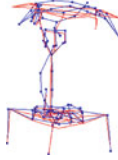
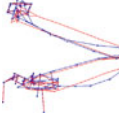
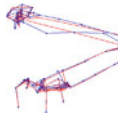
The flexibility of a pantograph is described by the experimental modes of vibration shown in Table 1 for the CX Pantograph [51]. The modal data acquisition is obtained by imposing a cyclical force to the pantograph head of constant value with frequencies ranging from 0 to 200 Hz. It is observed that important natural frequencies exist in the pantograph within the range of the operating frequencies of the overhead electric collection system, justifying that a flexible multibody approach is used to model the pantograph.

Several models of the pantograph, shown in Fig. 7, are modeled using a rigid-flexible multibody approach to evaluate their influence on the quality of the pantograph–catenary contact. The lower and top arms are steel tubular structures with varying cross-section, whereas the pantograph head is composed by steel, composite materials and carbon registration strips. Although highly detailed FEM models may be derived using solid and shell finite elements, simplified models of the referred bodies are used as local effect analysis as stress and strain analysis are not required. The mechanical data for the pantograph top arm and for its finite element model is shown in Table 2.

The modes of vibration of the top arm FEM model are obtained for free-free configuration, i.e., the model free in space. The first six structural natural frequencies are shown in Table 3.

The pantograph head, shown in Fig. 8, is another component for which the flexibility is expected to play a role. Its structure is composed by several elements with

**Table 1** Representative experimental modal basis of the CX Pantograph

Mode Frequency			Mode Frequency				
n°	(Hz)	Description		n°	(Hz)	Description	
1	11.0	Rotational movement of the main frame around base (Z)		2	19.3	Bending of the top link (Y)	
3	40.1	Bending of the lower link (Y)	X	4	45.7	Bending of the pantograph head (Z)	
5	49.3	Bending of the top arm (Z)		6	71.1	Bending of the top link (Z)	

**Fig. 7** CX pantograph used for the rigid-flexible multibody models

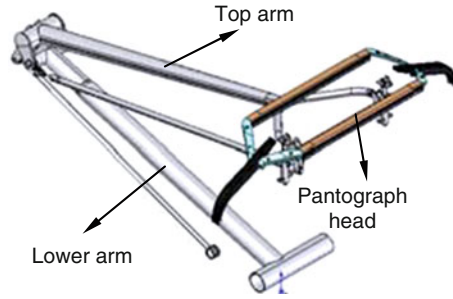


**Table 2** Material and geometric data for the upper arm and finite element information

Mechanical data	Unit	Value
Mass	[kg]	15.6
Young Modulus	[GPa]	206.8
Density	[kg/m <sup>3</sup> ]	7,820
Average length	[m]	1.36
FEM model data		Value
Finite element	[type]	3D elastic beam
Cross-section	[type]	Circular hollow
Cross-section area	[m <sup>2</sup> ]	$6.9 \times 10^{-4}$
Finite element		42
Nodes		43

different materials, including steel, for the support structures, carbon strips, for the registration strips, and composite materials, for the aerodynamic elements.

As the first mode of vibration of the pantograph head is a flexion mode, the structure may be modeled in a simple and straightforward way as a straight beam. The FEM model used is composed by a collection of beam elements, with rectangular cross-section and two lumped masses at the end-points of the straight beam, with the general characteristics shown in Table 4. The modes of vibration, for the free-free configuration, are described in Table 5.

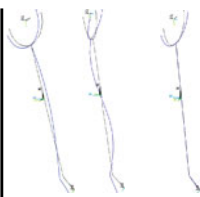
In order to appraise the influence of the flexibility of the top arm to the global dynamic behavior of the pantograph in the rigid-flexible pantograph multibody model only the top arm is described as a flexible body. Figure 9 shows a representation of this multibody model, referred to as pantograph model 2.

By considering the top arm as a flexible body, four virtual bodies are added to the multibody model to allow for the definition of kinematic joints. In Table 6, the main characteristics of the flexible multibody model are described.

The characteristics of the rigid bodies used in the multibody model are presented in Table 7 for the fully rigid multibody model. Note that the top arm is flexible and, consequently, the mass and inertia is not explicitly given as input data. The virtual bodies shown in Table 8, and added to the rigid multibody model, are in the points of the top arm involving kinematic joints.

**Table 3** Natural frequencies and modes of vibration of the FEM model of the top arm

Mode n°	Frequency		Description	n°	Mode	
	(Hz)	(Hz)			(Hz)	Description
1	89.9	100.8	First bending moment Z	2	100.8	First bending moment Y
3	219.9	276.1	Second bending moment Z	4	276.1	Second bending moment Y
5	358.5	383.8	Third bending moment Z	6	383.8	Forch opening







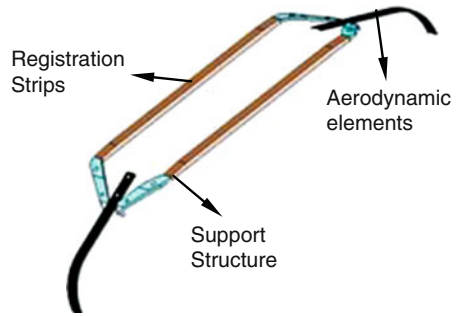




**Fig. 8** Pantograph head representation



**Table 4** Pantograph head FEM model characteristics

FEM model data	Unit	Value
Finite element		3D elastic beam
Cross-section		Rectangular
Cross-section area	[m <sup>2</sup> ]	5 × 10 <sup>-4</sup>
Finite element		2
Finite element		Lumped mass
Finite element		2
Nodes		3

**Table 5** Natural frequencies and modes of vibration of the pantograph head FEM model

Mode n°	Frequency (Hz)	Description		Mode n°	Frequency (Hz)	Description	
1	49.6	First bending moment X		2	98.7	Rotation X	
3	173.9	Second bending moment X		4	335.0	First bending moment Z	
5	398.7	Second rotation X		6	701.0	Translation + bending X	

The virtual bodies, 8 through 11, are linked to the flexible bodies through the rigid kinematic joints and to the rigid bodies through standard kinematic joints. Table 9 presents the definition of the rigid kinematic joints for the rigid-flexible pantograph multibody model 2. Note that the rigid-flexible joints rigidly attach a node of the flexible body mesh to a virtual body. Consequently, the mesh of the flexible body must be generated in such a way that at the least one node is included at each point

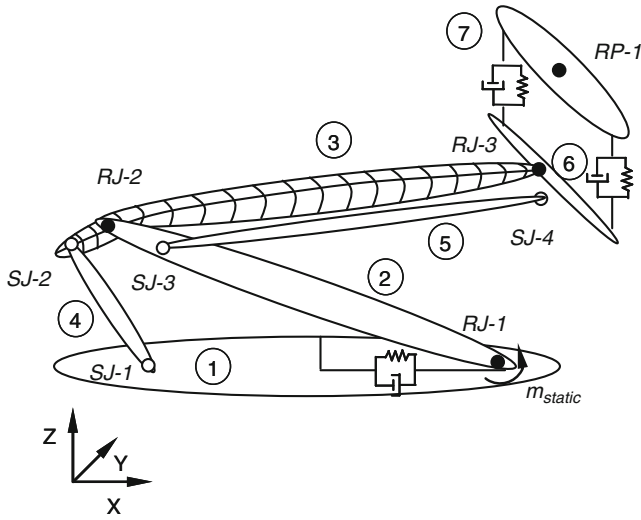


**Fig. 9** Pantograph model 2 with a flexible top arm

**Table 6** Characteristics of the pantograph multibody model 2

Multibody model data	Number
Rigid bodies	6
Virtual bodies	4
Flexible bodies	1
Rigid kinematic joints	8
Rigid-flexible kinematic joints	3

**Table 7** Rigid body data of the pantograph multibody model 2

ID	Rigid body	Mass (kg)	Inertia properties	Initial	Initial
			(kg.m <sup>2</sup> )	position (m)	orientation
			$I_{\xi\xi}/I_{\eta\eta}/I_{\zeta\zeta}$	$x_0/y_0/z_0$	$e_1/e_2/e_3$
1	Pantograph base	32.65	2.76/4.87/2.31	0.00/0.00/0.00	0.00/0.00/0.00
2	Lower arm	32.18	0.31/10.43/10.65	-0.57/0.00/0.41	0.00/0.17/0.00
3	Upper arm	15.6	0.15/7.76/7.86	-0.39/0.00/1.06	0.00/-0.18/0.00
4	Lower link	3.10	0.05/0.46/0.46	-0.89/0.00/0.28	0.00/0.21/0.00
5	Upper link	1.15	0.05/0.48/0.48	-0.36/0.00/1.00	0.00/-0.16/0.00
6	Stab. arm	1.51	0.07/0.05/0.07	0.55/0.00/1.42	0.00/0.00/0.00
7	Panto. head	9.50	1.59/0.21/1.78	0.55/0.00/1.51	0.00/0.00/0.00

to which a kinematic joint is attached. The linear force elements are detailed in Table 10. The force exerted by the air pump, located between the lower arm and the base of the pantograph, is represented as a constant moment  $n_\eta = 440$  Nm applied to the lower arm.

**Table 8** Data for the virtual bodies used in the flexible pantograph multibody model 2

ID	Rigid body	Mass (kg)	Inertia properties (kg.m <sup>2</sup> )	Initial position (m)	Initial orientation
			$I_{\xi\xi}/I_{\eta\eta}/I_{\zeta\zeta}$	$x_0/y_0/z_0$	$e_1/e_2/e_3$
8	Virtual body	0.0	0.0/0.0/0.0	-1.19/0.00/-0.13	0.00/-0.18/0.00
9	Virtual body	0.0	0.0/0.0/0.0	1.01/-0.31/0.00	0.00/-0.18/0.00
10	Virtual body	0.0	0.0/0.0/0.0	-1.01/0.00/0.00	0.00/-0.18/0.00
11	Virtual body	0.0	0.0/0.0/0.0	1.01/0.31/0.00	0.00/-0.18/0.00

**Table 9** Definition of the kinematic joints used in flexible multibody model 2

ID	Kinematic joint	Connected bodies		Attachment points Local coordinates (m)	
		i	j	Body $i$ ( $\xi_i/\eta_i/\zeta_i$ )	Body $j$ ( $\xi_j/\eta_j/\zeta_j$ )
1	Revolute joint	1	2	(0.02/0.00/0.13) <sub>P</sub> (0.02/1.00/0.13) <sub>Q</sub>	(0.82/0.00/0.00) <sub>P</sub> (0.82/1.00/0.00) <sub>Q</sub>
2	Revolute joint	2	10	(-0.82/0.00/0.00) <sub>P</sub> (-0.82/1.00/0.00) <sub>Q</sub>	(0.00/0.00/0.00) <sub>P</sub> (0.00/1.00/0.00) <sub>Q</sub>
3	Revolute joint	11	6	(0.00/0.00/0.00) <sub>P</sub> (0.00/1.00/0.00) <sub>Q</sub>	(0.00/0.31/0.00) <sub>P</sub> (0.00/1.31/0.00) <sub>Q</sub>
4	Spherical joint	1	4	(-0.26/0.00/0.00) <sub>P</sub>	(0.69/0.00/0.00) <sub>P</sub>
5	Spherical joint	8	4	(0.00/0.00/0.00) <sub>P</sub>	(-0.62/0.00/-0.03) <sub>P</sub>
6	Spherical joint	2	5	(-0.78/0.00/0.00) <sub>P</sub>	(-1.00/0.00/0.00) <sub>P</sub>
7	Spherical joint	5	6	(0.96/0.00/0.00) <sub>P</sub>	(0.00/0.00/-1.05) <sub>P</sub>
8	Spherical joint	9	6	(0.00/0.00/0.00) <sub>P</sub>	(0.00/0.00/-1.05) <sub>P</sub>
9	Rev.-prism. joint	6	7	(0.00/0.34/0.00) <sub>P</sub> (0.00/0.34/1.00) <sub>Q</sub>	(0.00/0.34/0.00) <sub>P</sub> (0.00/1.34/0.00) <sub>Q</sub>

**Table 10** Linear force elements data for the flexible multibody model 2

ID element	Linear force element	Spring elements		Damping coefficient (N.s/m)	Bodies		Attach points local coord (m)	
		Stiffness (N/m)	Length (m)		$i$	$j$	$\xi_i/\eta_i/\zeta_i$	$\xi_j/\eta_j/\zeta_j$
1	Spring-damper	2,000.00	9.06	3,000.00	1	2	0.28/0.00/0.09	0.82/0.00/-0.05
2	Spring-damper	3,600.00	0.12	13.00	6	7	0.00/0.34/0.00	0.00/0.34/0.00
3	Spring-damper	3,600.00	0.12	13.00	6	7	0.00/-0.34/0.00	0.00/-0.34/0.00

Another rigid-flexible pantograph multibody model, depicted as model 4 in Fig. 10 and described in Table 11, is used here considering the flexibility of the pantograph head only. The objective of this model is to understand the influence to the pantograph head on the quality of contact.

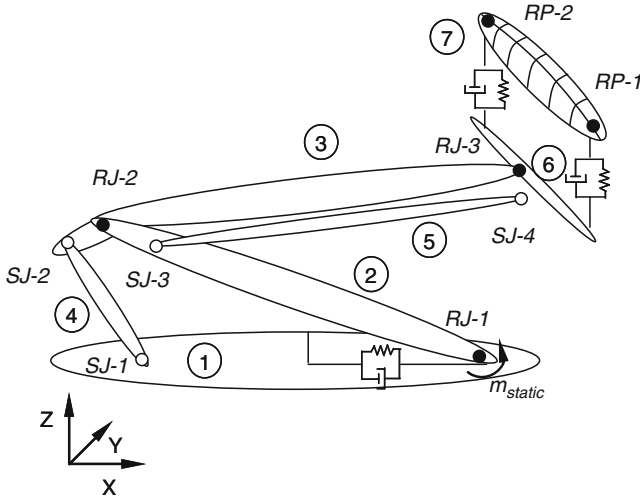


**Fig. 10** Pantograph model 4 with flexible head

**Table 11** Characteristics of the flexible pantograph head

Multibody model data	Number
Rigid bodies	6
Virtual bodies	4
Flexible bodies	1
Rigid kinematic joints	8
Rigid-flexible kinematic joints	4

**Table 12** Data for the virtual bodies in the rigid-flexible pantograph multibody model 4

ID	Rigid body	Mass (kg)	Inertia properties	Initial	Initial
			(kg.m <sup>2</sup> )	position (m)	orientation
			$I_{\xi\xi}/I_{\eta\eta}/I_{\zeta\zeta}$	$x_0/y_0/z_0$	$e_1/e_2/e_3$
8	Virtual body	0.0	0.0/0.0/0.0	0.55/0.34/1.51	0.00/0.00/0.00
9	Virtual body	0.0	0.0/0.0/0.0	0.55/-0.34/1.51	0.00/0.00/0.00
10	Virtual body	0.0	0.0/0.0/0.0	0.55/0.34/1.51	0.00/0.00/0.00
11	Virtual body	0.0	0.0/0.0/0.0	0.55/-0.34/1.51	0.00/0.00/0.00

In order to establish the kinematic constraints between the stabilization arm and the flexible pantograph head, four virtual bodies are used to establish a revolute-prismatic joint, to apply spring-dampers and to allow the application of the contact force. The positions of the virtual bodies, at the attachment locations of the kinematic joints, are shown in Table 12.

The virtual bodies are also used in order to handle all interactions between the flexible body and the surrounding environment, including forces generated by spring-damper elements or by contact. The rigid multibody model linear force element between the stabilization arm and the pantograph head are now set between the stabilization arm and virtual bodies.

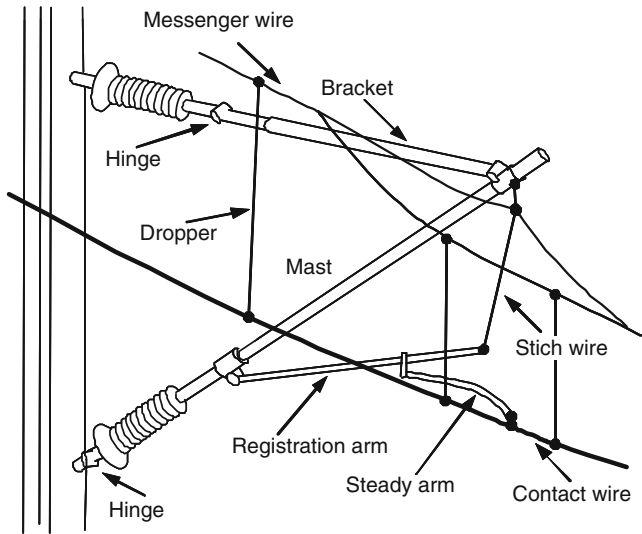


Fig. 11 Representation of a SNCF 25 kV suspended catenary

## 4.2 Catenary Finite Element Model

Catenaries are complex periodical structures, such as those presented in Fig. 11. Examples of typical structural elements involved in the catenary model are the contact, stitch and messenger wires, droppers and registration arms. Depending on the catenary system there are other elements that may have to be considered. In any case, the contact wire is the responsible for the contact between catenary and pantograph and therefore the element that provides electrical power. The messenger wire prevents excessive sag caused by the contact wire weight. Both of these wires are connected by vertical, tensile force droppers.

Even in a single European country there are different types of catenaries in use with different particularities in their construction. The contact wire is typically characterized by a small cross-section, compared to its length, being primarily suspended at the masts. Depending on the topology of the track and on the exposure to transversal winds the masts are placed at a distance of 27–63 m from each other. To maintain a constant mechanical stiffness of the contact wire a set of elements are designed to suspend the contact wire at these locations, specific of each suspended catenary type. In the French 25 kV catenary represented in Fig. 11 the contact wire is suspended by a low inertial elemental called the steady arm which is linked to the registration arm. The latter is suspended with respect to the messenger wire by the stitch wire and is connected by a hinge to the mast. This solution aims at limiting the dynamic coupling between the contact wire and the supporting elements. To minimize the spatial curve described by the contact wire and to maximize the wave propagation velocity of the contact wire a static load is applied to its extremities.

If seen from the top, the contact wire is suspended forming a *zigzag* around the longitudinal direction, designated by stagger. This geometric characteristic of the suspended catenary enables a constant wear of the pantograph registration strip.

### 4.3 Simulation Scenario and Results

To be able to understand the influence of the flexibility of the structural elements of the pantograph on the contact dynamics of the pantograph–catenary interface a single pantograph scenario is analyzed. The scenario corresponds to a single pantograph system attached to a railway vehicle running at approximately 300 km/h on a straight track, as depicted in Fig. 12.

The flexible multibody model 2 allows the analysis of the deformation of the upper arm. As expected the deformation is described by the bending modes of vibration. The results depicted in Fig. 13 show that the dominant mode of vibration on the pantograph top arm behavior is the first bending mode.

The bending of the upper arm results in lowering the position of the contact points with the pantograph head, as depicted in Fig. 14. However, the differences observed on the contact kinematics are not reflected on the contact forces, which are similar for the rigid and flexible models as seen in Fig. 15.

The analysis of the influence of pantograph head deformation in the contact force generated due to the pantograph–catenary interaction is analyzed also. Disregarding the deformation of the main frame can be, it is possible to understand the influence of the flexibility of the pantograph head by modeling the pantograph using the flexible multibody model 4. As depicted in Fig. 16, the first and second bending modes contribute to the deformation of the pantograph head. The deformation of the pantograph head has a very small influence on the contact forces, as seen in Fig. 17.

Although, for operational conditions and considering the present catenary model the influence of the deformation of the pantograph head may be disregarded without loss of accuracy, its influence is important to develop an actively controlled pantograph. Another aspect not studied in this work is the effect of the pantograph

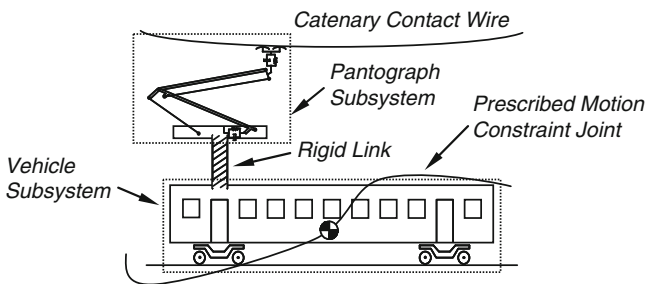


Fig. 12 Scenario for a high-speed train equipped with a pantograph running on a tangent track